

## Fabrication and Investigation of Graphene-Rubber Nanocomposite Based Multifunctional Flexible Sensors

Muhammad Tariq Saeed Chani<sup>1,2</sup>, Khasan S. Karimov<sup>3,4</sup>, Essra M. Bukhsh<sup>1</sup>, Abdullah M. Asiri<sup>1,2</sup>

<sup>1</sup> Chemistry Department, Faculty of Science, King Abdulaziz University, Jeddah 21589, P.O. Box 80203, Saudi Arabia

<sup>2</sup> Center of Excellence for Advanced Materials Research, King Abdulaziz University, Jeddah 21589, P.O. Box 80203, Saudi Arabia

<sup>3</sup> Ghulam Ishaq Khan Institute of Engineering Sciences and Technology, Topi-23640, District Swabi, KPK, Pakistan

<sup>4</sup> Center for Innovative Development of Science and New Technologies of Academy of Sciences of Tajikistan, Dushanbe, 734025, Rudaki 33, Tajikistan

\*E-mail: [tariqchani1@gmail.com](mailto:tariqchani1@gmail.com)

Received: 8 February 2020 / Accepted: 3 April 2020 / Published: 10 May 2020

This study presents the design, fabrication, investigation and properties of the elastic multifunctional sensors based on graphene-rubber nanocomposite. The sensors are sensitive to stretching force, acceleration and temperature. The sensors were fabricated using pressing-sliding (or rubbing-in) technology. In the process of fabrication, the graphene powder was penetrated in (built-in) bulky rubber substrate forming the solid nanocomposite. The change in DC resistance and impedance (at a frequency of up to 200 kHz) of the samples were measured in the temperature interval of 26–60 °C. The effects of stretching force (up to 19 gf) and acceleration (up to 19 m/s<sup>2</sup>) were also investigated and it was found that in both cases the resistance and the impedance decreased by 14% and 16%, accordingly. Under the normal conditions, by changing the temperature from 26 to 60 °C the resistance and the impedance were changed by 35% and 28%, respectively. These changes of the investigated parameters of the sensors under the effect of force and acceleration may be, firstly, due to the increasing distances between particles of graphene in the composite. Secondly, it may be due to changing of the intrinsic properties of the particles and rubber under the effect of the temperature on the nanocomposite.

**Keywords:** Rubbing-in; Resistance; Impedance; Accelerometer; Stretching; Pressure sensing.

### 1. INTRODUCTION

During last years, number of flexible devices have been developed and fabricated. The microfluidic flexible device for the characterization of mechanical properties of the viscoelastic (soft)

solids like bacterial biofilms was fabricated and investigated [1]. The ref. [2] presented the properties of a graphene oxide based flexible device for resistive memory switching. A multilayer metal/polymer based flexible device for sensing of contact force in robotics was described in ref. [3]. In ref. [4] a carbon nanofiber sheet (nanocomposite) based field emission flexible device was discussed. A polyethylene terephthalate based electroluminescent flexible device was produced and tested using transparent CNTs electrodes [5] and a display based on flexible OLED (organic light-emitting diode) was described in ref. [6].

Except of flexibility for practical applications, first of all, the fabrication and investigation of multifunctional devices are important. Moreover, the devices are needed for the development of concerned technology and as a teaching aid for the new generation of researches. Analysis of electrical and mechanical properties of the devices can be used for the selection of sensors, and in particularly force and acceleration sensors [7]. A novel flexible piezoresistive device containing graphite based sensing component was demonstrated in ref. [8]. The fabrication of these devices was simple and fast. The ref. [9] presented the accelerometer fabricated on the base of paper which was coated by a piezoelectric ZnO-nanopowder.

Ref. [10] discussed the use of accelerometers near to robotic manipulators' end-effectors to improve their force-control performance. An observer approach model was proposed which was based on the fusion of information from different types of sensors. By system identification a model was devised for the robot-grinding tool having new sensors. For improvement verification an impedance-control scheme was suggested. It was considered that the selection of sensors should be done by realization of the matching of the properties and characteristics of the sensors to the requirements of an applications. Ref. [11] described fabrication of paper-based MEMS piezoresistive force sensors, where the patterning of conductive materials was done on a paper substrate. The performance of these sensors to measure the forces was moderate. A weight balance with 15 g measuring range and 25 mg resolution was also fabricated on paper. In ref. [12] a novel structured angular-acceleration sensor working on electromagnetic induction principle was designed and fabricated. These sensors were based on constant magnetic field (produced sensor's excitation windings of sensor) and a rotor (cup-shaped) which cut the magnetic field. An electromotive force generated by the sensor's output windings was directly proportional to the acceleration (angular) generated by electromagnetic coupling.

In ref. [13] the flexure of semiconductor mass supporting semiconductor beams was measured by a silicon accelerometer using single-crystal silicon's piezoresistive effect. A Wheatstone bridge was used to connect these piezo resistors to get a symmetric differential-output [14]. In refs. [15, 16] described the design, fabrication and utilization of the flexible strain sensors for the investigation of the conductive polymer composite-based textile structures and the *in-situ* measurement of deformation in parachute canopy. The effect of bending on the properties of the flexible thin film transistors was investigated in ref. [16]. Ref. [17] devised a new technique to measure gravity-based acceleration and investigate the free-falling object's dynamics using a simple and low-cost setup. To estimate the gravity-based acceleration the freely passing IR (infrared) transceiver was used. During the measurement of free-falling time of object, the IR transceiver is used to deduce gravity-based acceleration. By fitting measured elapsed falling times to the quadratic equation of motion under constant acceleration, the correct value of gravity-based acceleration  $g = 9.8092 \pm 0.0384 \text{ m s}^{-2}$  was obtained.

A strain gauge for the measurement of displacement was fabricated and investigated by us [18]. A CNTs composite-based flexible capacitance and impedance tensile load sensor was discussed in ref. [19]. A novel pressure and displacement sensors based on carbon nanotubes was presented in ref. [20]. The transversal tensile resistive effect in TEA ( $\text{TCNQ}_2$ ) crystals was studied [21] and ref. [22] investigated the displacement sensitive OFET (organic field effect transistor) for application in telemetry system.

In this paper, in continuation of our efforts for the fabrication and investigation of the organic materials based electronic devices [23-37] we are presenting the fabrication and investigation of the multifunctional temperature, stretching force and acceleration sensors. The graphene and rubber were used for fabrication of the nanocomposite.

## 2. EXPERIMENTAL

For the fabrication of the temperature, stretching force and acceleration elastic bulky sensors based on graphene and rubber composite the graphene powder and hollow rubber substrates were used. The outer length and the width of the elastic rubber substrates were equal to 3cm and 2cm, accordingly, while the depth was equal to 1 cm.

For the fabrication of sensors, the rubber substrates were fixed on the solid platform at room temperature. By the pressing-sliding (or rubbing-in) technology the graphene powder was penetrated (built-in) into the surface of the substrates (Fig.1 shows side view). During this process the pressure on the graphene powder was equal to  $30\text{-}40 \text{ gf/cm}^2$ . As a result, a  $20\text{-}30 \mu\text{m}$  thick solid graphene-rubber composite film was formed. Optical microscope image of the graphene on rubber sample was acquired using an Olympus metallurgical microscope having digital camera (built-in camera). The optical micrograph is shown in the Fig. 2.

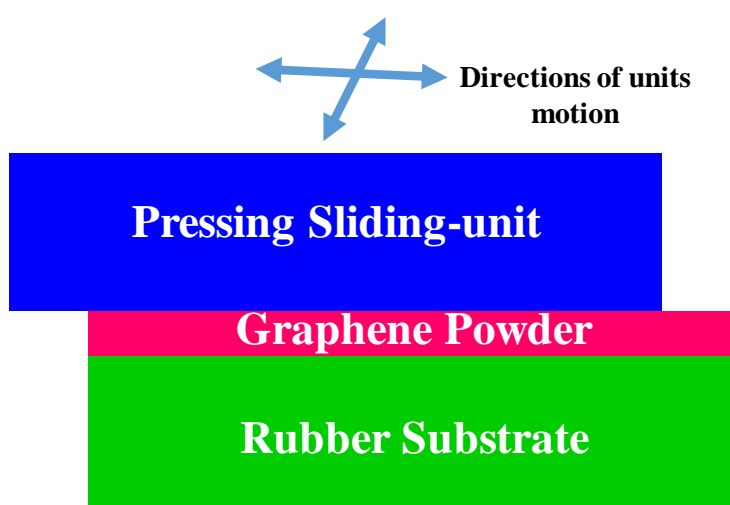


**Figure 1.** Illustration of the pressing-sliding (or rubbing-in) process to fabricate the graphene-rubber composite film.

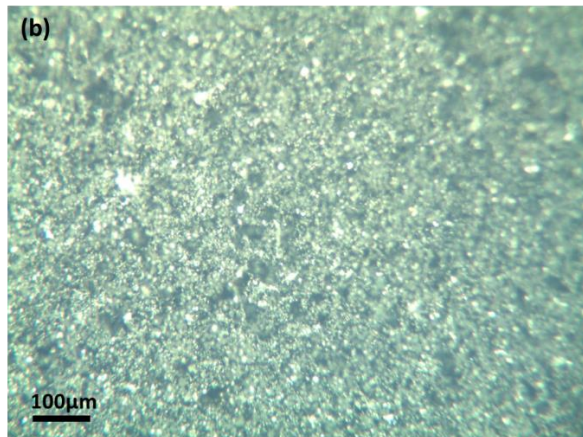


**Figure 2.** Optical micrograph of the graphene built-in rubber composite.

The front view, side view and top view of the graphene-rubber composite film based multifunctional temperature, stretching force and acceleration sensor are shown in Fig. 3a, 3b and 3c, respectively. Figure 3d shows the schematic diagram (side view) of the sensor with sensor holder and applied force. The sensor consists of rectangular hollow elastic rubber substrate, graphene-rubber nanocomposite thin film and conductive terminals. The weights, in Fig.3d (Force) were used for the calibration of the sensor. The outer length and the width of the elastic rubber substrate were equal to 3 cm and 2 cm, accordingly, while the depth was equal to 1 cm.

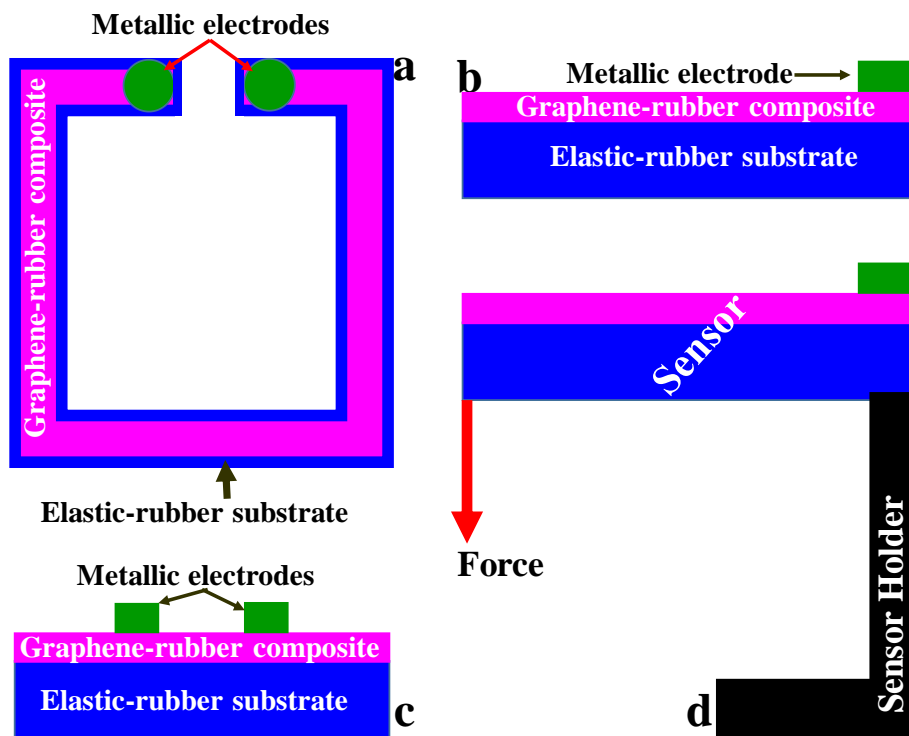


**Figure 3.** The front view (a), side view (b) and top view (c) of the fabricated sensor, and the schematic diagram (side view) of the sensor with sensor holder and applied force (d).

The multifunctional sensors which were tested for the measurement of force (Fig.3) can also be used for the measurement of the acceleration. Acceleration (a) was estimated by use of the following expression:

$$a = F/m \quad (1)$$

where,  $F$  is force,  $m$  is sum of the fixed initial mass and variable mass accordingly. If the sensor is loaded, the mass will increase respectively. Accordingly, the resistance of the sensor due to stretching effect increases. Changing of total mass allows to get different values of the sensor's resistance, which would be proportional to the values of acceleration if it would be measured directly.

For the measurements of temperature, the TECPEL 322 multimeter was used, while the resistance and impedance were measured by MT 4090 LCR meter. The force was created by using calibrated weights.

### 3. RESULTS AND DISCUSSION

The resistances and the impedances of the graphene-rubber nanocomposite-based multifunctional flexible sensors were investigated under the effect of heating, stretching force and acceleration.

The effects of temperature on the DC resistance ( $R$ ) and impedance (at frequencies 100 Hz to 200 kHz) of the sensors are shown in Fig.4a and 4b, respectively.

It may be seen that the increase of temperature in the range of 26 to 60 °C causes to decrease the resistance and impedance of the sensor. This decrees in resistance or impedance with increase in temperature may be explained by the percolation theory where it is considered that the conduction mechanism is based on transition between two spatially separated particles or sites. As per percolation theory the conductivity of the film is inversely proportional to the characteristic length and path resistance. On increasing temperature, the charge carriers generate due to the heating of composite layer that in turn reduce the path resistance. Moreover, the graphene-rubber composite may be squeezed because of thermal expansion and results in reduction of resistance by increasing sample's effective cross-section or increasing contact area between the particles [38-41]. It is also evident from the Fig. 4 that the resistance-temperature and the impedance-temperature relationships are linear. The temperature coefficients of the resistance ( $TCR$ ) and impedances ( $TCZ$ ) can be estimated by the following relationships:

$$TCR = dR/RdT \quad (2)$$

$$TCZ = dZ/ZdT \quad (3)$$

Where,  $R$  is the initial resistance and  $Z$  is the initial impedance. The  $dR$ ,  $dZ$  and  $dT$  are change in resistance and change in impedance and change in temperature, respectively.

In some approximation for the simulation of the experimental data the linear function can be used:

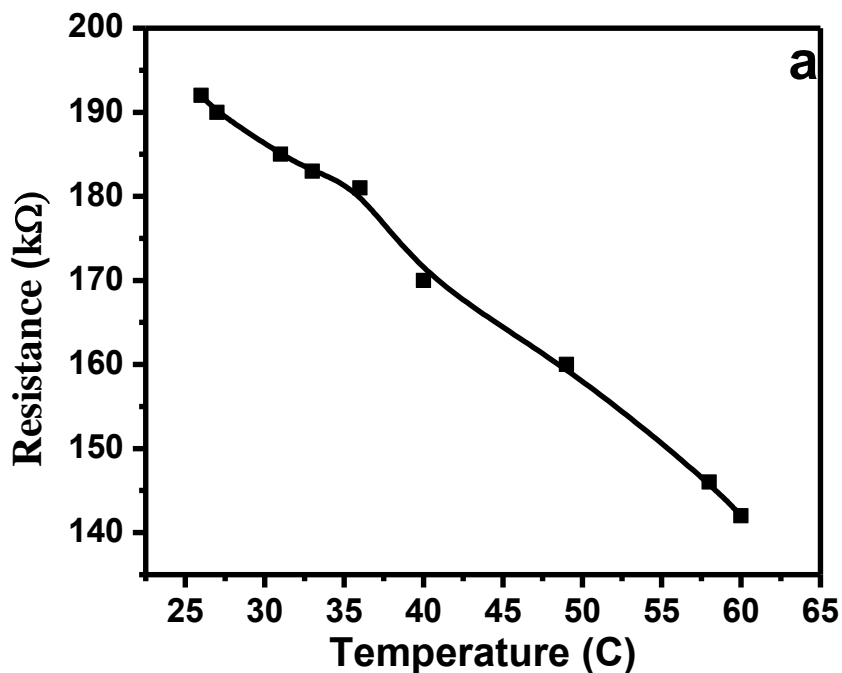
$$Y = ax + b \quad (4)$$

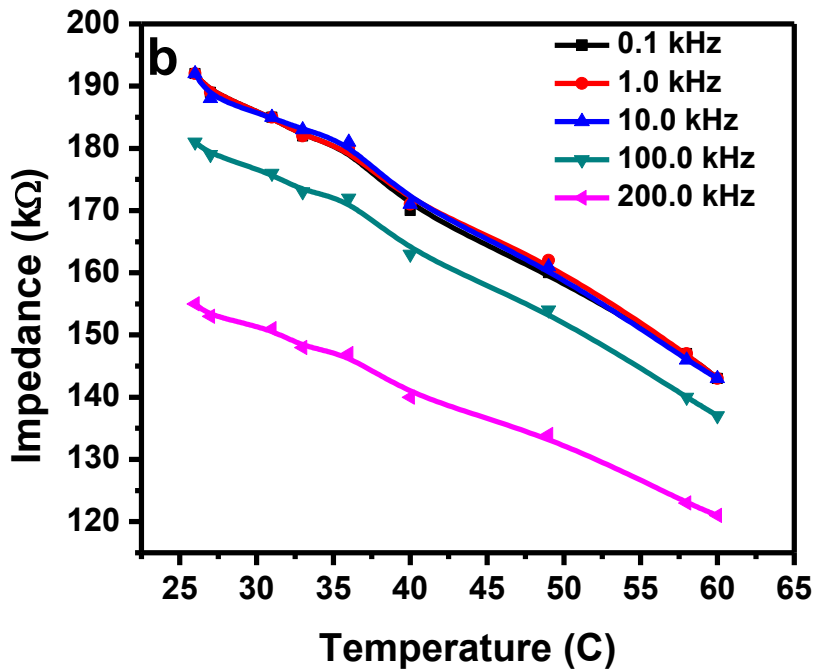
At linear approximation of the experimental graphs (Fig.4), it can be found that  $TCR$  is equal to  $0.00765 \text{ C}^{-1}$  and  $TCZ$  for  $Z$  (200 kHz) is equal to  $0.00645 \text{ C}^{-1}$ .

The experimental data, particularly the data related to impedance  $Z$  (100 Hz) and temperature relationships shown in Fig.4 can be represented by the following equation:

$$Z_{(100)} = -1.44 \left( \frac{k\Omega}{^{\circ}\text{C}} * \Delta T (^{\circ}\text{C}) \right) + 203 \text{ (k}\Omega\text{)} \quad (5)$$

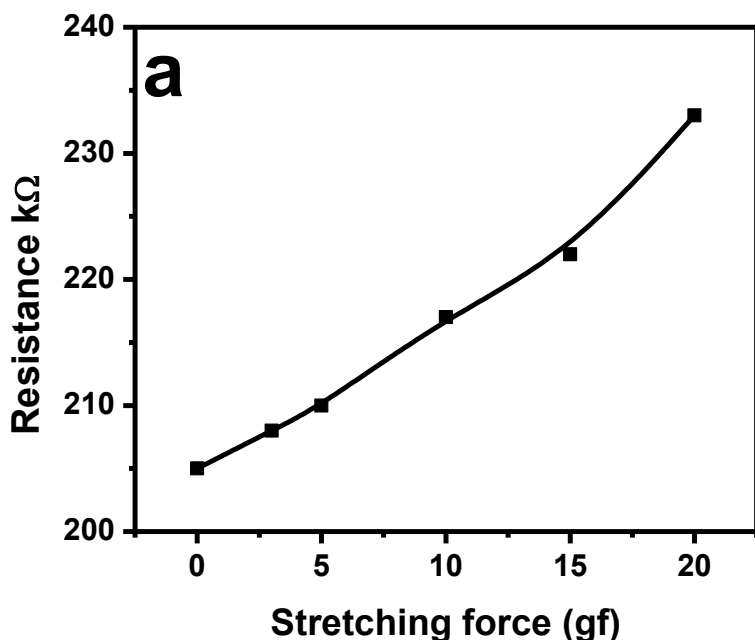
The temperature dependences of the graphene and graphene composites were investigated in a several research studies. Ref. [42] reported the fabrication of GNPs (graphene nanoparticles) based temperature sensor. It was observed that the temperature variation of resistance was linear in the range of  $10\text{--}60\text{ }^{\circ}\text{C}$  and it can be selected for the sensor application. The  $TCR$  (temperature coefficient of resistance) was equal to  $0.0371$ . The presented  $TCR$  is positive and higher than the  $TCR$  value ( $0.0075 \text{ C}^{-1}$ ) obtained by us. Moreover, the value of  $TCR$  is negative in our case. It is definitely due to the differences in the composition and structures of our sensors and the sensors described in ref. [42]. At the same time both results are higher than that of multiwall carbon nanotubes presented in ref. [43] as well. Though a small hysteresis was observed, but it was considered that the sensors have potential to apply as a highly sensitive and fast-response temperature sensors [43]. It could be mentioned that at present, graphene is used for drug testing in the biochemical sensors [43] and for monitoring of gas [44].





**Figure 4.** Effects of temperature on the DC resistance (a) and impedance (b) of the graphene-rubber nanocomposite based multifunctional sensors.

The stretching force ( $P$ ) sensing properties of the sensors are presented in Fig.5. It may be seen that, as the stretching force increases the resistance (Fig. 5a) and impedances (Fig. 5b) also increase. Obviously, under the effect of stretching force the elastic deformation takes place in the sensor which results in increase in the length and decrease in the width of sensor. This deformation causes the increase in resistance of the sensor. The sensor was calibrated with standard weights in the range of 0-20 gf.



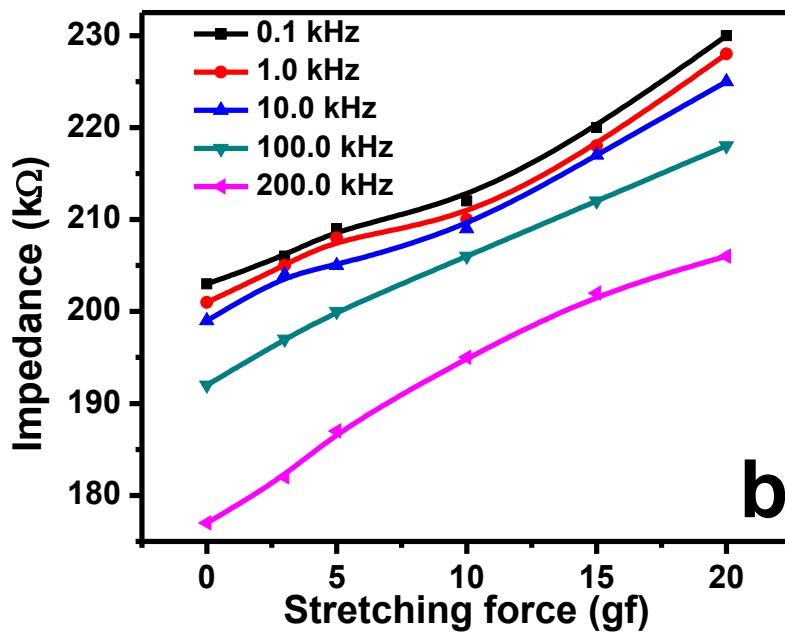


**Figure 5.** The resistance-stretching force (a) and the impedance-stretching force (b) relationships obtained experimentally at direct and alternating currents, respectively.

The stretching force coefficients of resistance ( $PCR$ ) and the impedance ( $PCZ$ ) of the graphs shown in Fig.5 represent the sensitivity of the force sensors, can be estimated by the following relationships:

$$PCR = \frac{dR}{RdP} \quad (6)$$

$$PCZ = \frac{dZ}{ZdP} \quad (7)$$

Where,  $dP$  is the change in stretching force. The calculated values of the graph's slopes were equal to  $6.83 \cdot 10^{-3} \text{ gf}^{-1}$ ,  $6.65 \cdot 10^{-3} \text{ gf}^{-1}$ ,  $6.71 \cdot 10^{-3} \text{ gf}^{-1}$ ,  $6.77 \cdot 10^{-3} \text{ gf}^{-1}$ ,  $6.79 \cdot 10^{-3} \text{ gf}^{-1}$  and  $6.90 \cdot 10^{-3} \text{ gf}^{-1}$ , accordingly at DC, 100 HZ, 1 kHz, 10kHz, 100 kHz and 200 kHz. Physically, the relationships shown in Fig.5 can be explained by increasing distance between graphene particles in the composite under the influence of stretching force. At the same time the changes of the intrinsic properties of the particles in the graphene-rubber composite may take place in some extend. The increase in frequency results in increase in contribution of reactive conduction, due to the presence of the capacitive component in the impedance. In turn probably it is responsible for the decrease in impedance. These physical properties of the sensors can be explained if it is considered that the equivalent circuit of the sensor has the parallel connection of the resistance and capacitance.

The impedance and stretching force (e.g. at 100 Hz) relationship can be described by the following expression based on experimental data:

$$Z_{(100)} = 1.35 \left( \frac{k\Omega}{gf} * P(gf) \right) + 203 \text{ (k}\Omega\text{)} \quad (8)$$

Related to the mechanical properties, in particular, the effect of strength was investigated in graphene oxide/polyvinyl alcohol composites that were suggested for use as a promising biomaterial in

tissue and biomedical engineering. But their development was hindered because of poor water-retention and mechanical properties [45].

A graphene-based novel optical MEMS accelerometer was fabricated and it was reliant on graphene's optical properties and intensity modulation [46]. The accelerometer's sensing system was comprised of a light source, multilayer graphene finger, photodiode, laser diode, and integrated optical waveguides. The simulation based functional characteristics of accelerometer were the following: the mechanical sensitivity of 1,019 nm/g, an optical sensitivity of 145.7 %/g, a resonance frequency of 15,553 Hz, a bandwidth of 7 kHz, and a measurement range of  $\pm 10$  g.

Along with force the measurement of acceleration is very wide used in practice. Looking forward for the development of accelerators technology we designed, fabricated and tested a simple and sensitive accelerometer. Fig.6 shows the acceleration-impedance relationship at different frequencies (100 Hz, 100k Hz and 200 kHz). As the acceleration increases the impedances increases as well. The reason of increasing impedance with increase in acceleration is like that of previous case: the acceleration is proportional to the force; the stretching force causes to the increase the distances between graphene particles in the composite and resultantly the impedance increases. It turns the impedance increases due to the increase of resistive components and decrease of the capacitive components that finally results to increase the impedance. As the frequency increases the impedances decreases due to the presence of the capacitive component in the impedance. The acceleration coefficients of impedance (ACZ), which represent the sensitivity of the acceleration sensors can be estimated by the following relationship:

$$ACZ = \frac{dZ}{ZdA} \quad (9)$$

Where,  $A$  is the acceleration,  $Z$  is the impedance and  $dZ$  and  $dA$  are the change in impedance and change in acceleration, respectively. The slopes which characterize the sensitivity are calculated, which are equal to  $0.00648 \text{ s}^2/\text{m}$ ,  $0.00433 \text{ s}^2/\text{m}$  and  $0.0167 \text{ s}^2/\text{m}$ , accordingly at the frequencies of 100 Hz, 100 kHz and 200 kHz.

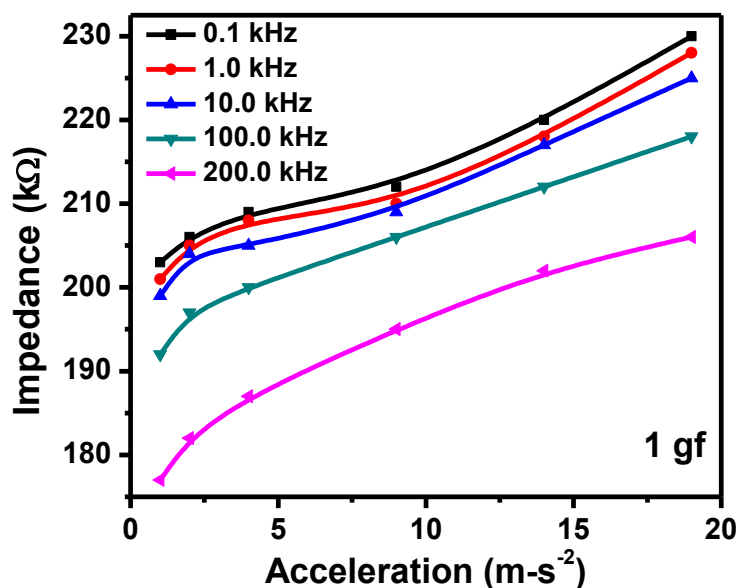


**Figure 6.** Acceleration-impedance relationship of the graphene-elastic rubber composite based multifunctional sensors.

The acceleration-impedance relationship can be represented by the following equation.

$$Z_{(100)} = 1.38 \left( \frac{k\Omega}{m/s^2} * A(m/s^2) \right) + 203 (k\Omega) \quad (10)$$

The investigation of force, acceleration and temperature sensor based on graphene-elastic rubber nanocomposite thin film allows to fabricate multifunctional sensors which may be used in many areas of instrumentation technology. In ref. [47] the wearable multifunctional printed graphene sensors were described. The developed wearable resistive bending sensors can be used for the measurement of force, deflection, and curvature. In the review article [48] presented the results of measurements of several parameters as: heart rate, body temperature, pulse oxygenation, blood pressure, respiration rate, blood glucose, electroencephalograph signal, electromyogram signal and electrocardiogram signal. These parameters are important for the estimation of health conditions. The new graphene-based health monitoring sensors were discussed in detail in terms of structures, sensor systems components, technological innovations, sensing mechanisms and potential challenges. Ref. [49] presented the fabrication of a simple and low cost graphene sensor (laser-induced) for multi-sensing. The graphene was synthesized by the LASER irradiation of commercial polymer and used to fabricate capacitive electrochemical and strain sensors. A graphene oxide (reduced) film based wearable multifunctional sensor fabricated on the porous film of inverse opal-acetyl-cellulose (IOAC) [50], which is used simultaneously for the monitoring (*in-situ*) of sweat (ion concentration) and different human motions. The graphene oxide film acts as a strain sensor and monitors the human motion through resistant variation. The IOAC flexible film acts not only as a motion sensor but also an excellent ion collector and analyzer (ions in sweat). These devices can monitor various human motions such as wrist bending, finger bending, head rotation and the throat movement. In ref. [51] it was presented the investigation of recent development for flexible pressure sensors, trends of wearable flexible-sensors and E-skin, multi-function equipment, exploration of new functional-materials and sensing mechanisms, emerging new integration-technology of flexible devices which will be the important directions in the future sensors technology.

The rubbing-in technology can be realized easier if two materials are selected properly on the base of work functions. In electrochemistry the selection of materials is also realized according to work function (or electrochemical potential). Therefore, the process which take place in rubbing-in technology and electrochemistry have some similarities from this point of view. More detailed information is available in the following articles [52, 53].

The information presented in this paper showed that at present the graphene-based sensors cover very wide area of the devices for measurement of environmental, industrial and technological parameters [42, 43, 45-48] and this process is continued. In ref. [54] by us an elastic layered bulky rubber-graphene composite was developed to fabricated multi-functional sensors by rubbing-in technology. The effects of compressive displacement, temperature, humidity and pressure on the sensor's impedance were investigated. Under the effect of displacement (compressive) and pressure the impedance of sensors decreased. These flexible rubber-graphene composite maybe used potentially as a frequency, displacement, pressure and temperature sensors [51].

#### 4. CONCLUSION

Comparison of the data which were published in literature with presented in this paper showed that the experimental results, first of all, can be used for the development of technology of multifunctional sensors and, in particular, in this area of electronic devices and instrumentation. The sensors are sufficiently sensitive, due to use of graphene and rubber substrate, earthy and simple for fabrication, cheap and reliable that is important for use in practice. Further investigations and especially study of aging processes in the devices would be useful for the application of the investigated sensors. Recent publications [43, 48, 50, 54, 55] shows that researchers are interested to investigate graphene and graphene-based complexes from the point of optimizing technology, physical processes, and potentially fabrication of reliable, sensitive and low-cost electronic devices.

#### ACKNOWLEDGEMENT

This project was funded by Saudi Arabia Basic Industries Corporation (SABIC) and the Deanship of Scientific Research (DSR) at King Abdulaziz University, under grant no. S-37-130-40. The authors, therefore, acknowledge with thanks SABIC and DSR for technical and financial support.

#### References

1. D. N. Hohne, J. G. Younger, M. J. Solomon, *Langmuir*, 25 (2009) 7743.
2. S. K. Hong, J. E. Kim, S. O. Kim, S. Choi, B. J. Cho, *IEEE Electron Device Letters*, 31 (2010) 1005.
3. E.-S. Hwang, Y.-R. Yoon, H.-R. Yoon, T.-M. Shin, Y.-J. Kim, *Sensors and Materials*, 20 (2008) 55.
4. M. Kawamura, Y. Tanaka, T. Kita, O. Wada, H. Nakamura, H. Yanagi, A. Magario, T. Noguchi, *Applied Physics Express*, 1 (2008) 074004.
5. M. J. Kim, D. W. Shin, J.-Y. Kim, S. H. Park, I. t. Han, J. B. Yoo, *Carbon*, 47 (2009) 3461.
6. S. Kim, H.-J. Kwon, S. Lee, H. Shim, Y. Chun, W. Choi, J. Kwack, D. Han, M. Song, S. Kim, S. Mohammadi, I. Kee, S. Y. Lee, *Advanced Materials*, 23 (2011) 3511.
7. J. Shieh, J. E. Huber, N. A. Fleck, M. F. Ashby, *Progress in Materials Science*, 46 (2001) 461.
8. T.-L. Ren, H. Tian, D. Xie, Y. Yang, *Sensors*, 12 (2012) 6685.
9. Y.-H. Wang, P. Song, X. Li, C. Ru, G. Ferrari, P. Balasubramanian, M. Amabili, Y. Sun, X. Liu, *Micromachines (Basel)*, 9 (2018) 19.
10. J. G. Garcia, A. Robertsson, J. G. Ortega, R. Johansson, in *2004 IEEE/RSJ International Conference on Intelligent Robots and Systems (IROS) (IEEE Cat. No.04CH37566)*. (2004), vol. 3, pp. 3009.
11. X. Y. Liu, M. O. Brien, M. Mwangi, X. J. Li, G. M. Whitesides, in *2011 IEEE 24th International Conference on Micro Electro Mechanical Systems*. (2011), pp. 133.
12. H. Zhao, H. Feng, *Sensors (Basel)*, 13 (2013) 10370.
13. J. I. D. Hansson, TX). (Texas Instruments Incorporated (Dallas, TX), United States, 1985).
14. C. Cochrane, V. Koncar, M. Lewandowski, C. Dufour, *Sensors (Basel)*, 7 (2007) 473.
15. C. Cochrane, M. Lewandowski, V. Koncar, *Sensors (Basel)*, 10 (2010) 8291.
16. J.-M. Kim, T. Nam, S. J. Lim, Y. G. Seol, N. E. Lee, D. Kim, H. Kim, *Applied Physics Letters*, 98 (2011) 142113.
17. S. AbdElazem, W. Al-Basheer, *European Journal of Physics*, 36 (2015) 045017.

18. K. S. Karimov, R. Patent, Ed. (Russia, 1991), chap. 2019788.
19. Z. Ahmad, K. S. Karimov, F. Touati, *Chinese Physics B*, 25 (2016) 028801.
20. K. S. Karimov, K. Sulaiman, Z. Ahmad, K. M. Akhmedov, A. Mateen, *Chinese Physics B*, 24 (2015) 018801.
21. K. S. Karimov, *Synthetic Metals*, 44 (1991) 103.
22. K. S. Karimov, T. A. Qasuria, *Measurement*, 45 (2012) 41.
23. M. T. S. Chani, *Microchimica Acta*, 184 (2017) 2349.
24. M. T. S. Chani, A. M. Asiri, K. S. Karimov, M. Bashir, S. B. Khan, M. M. Rahman, *International Journal of Electrochemical Science*, 10 (2015) 3784.
25. M. T. S. Chani, A. M. Asiri, K. S. Karimov, A. K. Niaz, S. B. Khan, K. A. Alamry, *Chinese Physics B*, 22 (2013) 118101.
26. M. T. S. Chani, K. S. Karimov, A. M. Asiri, *Journal of Materials Science: Materials in Electronics*, 30 (2019) 6419.
27. M. T. S. Chani, K. S. Karimov, A. M. Asiri, *Semiconductors*, 53 (2019) 1622.
28. M. T. S. Chani, K. S. Karimov, A. M. Asiri, N. Ahmed, M. M. Bashir, S. B. Khan, M. A. Rub, N. Azum, *PloS one*, 9 (2014) e95287.
29. M. T. S. Chani, K. S. Karimov, F. A. Khalid, K. Raza, M. U. Farooq, Q. Zafar, *Physica E*, 45 (2012) 77.
30. M. T. S. Chani, K. S. Karimov, S. B. Khan, A. M. Asiri, *Sensors and Actuators A*, 246 (2016) 58.
31. M. T. S. Chani, K. S. Karimov, S. B. Khan, A. M. Asiri, M. Saleem, M. M. Bashir, *Optoelectronics and Advanced Materials Rapid Communications*, 7 (2013) 861.
32. M. T. S. Chani, K. S. Karimov, S. B. Khan, N. Fatima, A. M. Asiri, *Ceramics International*, 45 (2019) 10565.
33. M. T. S. Chani, K. S. Karimov, H. Meng, K. M. Akhmedov, I. Murtaza, U. Asghar, S. Z. Abbass, R. Ali, A. M. Asiri, N. Nawaz, *Russian Journal of Electrochemistry*, 55 (2019) 1391.
34. M. T. S. Chani, S. B. Khan, A. M. Asiri, K. S. Karimov, M. A. Rub, *Journal of the Taiwan Institute of Chemical Engineers*, 52 (2015) 93.
35. M. T. S. Chani, S. B. Khan, K. S. Karimov, A. M. Asiri, K. Akhtar, M. N. Arshad, *International Journal of Electrochemical Science*, 10 (2015) 10433.
36. M. T. S. Chani, K. S. Karimov, J.-u. Nabi, M. Hashim, I. Kiran, A. M. Asiri, *International Journal of Electrochemical Science*, 13 (2018) 11777.
37. M. T. S. Chani, K. S. Karimov, A. M. Asiri, *International Journal of Electrochemical Science*, 12 (2017) 1434.
38. K. S. Karimov, M. T. S. Chani, F. A. Khalid, *Physica E*, 43 (2011) 1701.
39. M. T. Saeed, PhD Thesis, *GIK Institute of Engineering Sciences and Technology*, (2012).
40. M. T. Saeed, K. S. Karimov, F. A. Khalid, M. Farooq, M. Saleem, in *2011 Saudi International Electronics, Communications and Photonics Conference (SIECPC)*. (IEEE, 2011), pp. 1.
41. K. S. Karimov, F. Khalid, M. Chani, A. Mateen, M. A. Hussain, A. Maqbool, J. Ahn, *Optoelectronics and Advanced Materials Rapid Communications*, 6 (2012) 194.
42. L. Zhang, Z. Wang, C. Xu, Y. Li, J. Gao, W. Wang, Y. Liu, *Journal of Materials Chemistry*, 21 (2011) 10399.
43. M. Ahmadian, K. Jafari, M. J. Sharifi, *ETRI Journal*, 40 (2018) 794.
44. M. Tian, Y. Huang, W. Wang, R. Li, P. Liu, C. Liu, Y. Zhang, *Journal of Materials Research*, 29 (2014) 1288.
45. H. Wu, L. T. Drzal, *Carbon*, 50 (2012) 1135.
46. P. Yan, Q. Tang, A. Deng, J. Li, *Sensors and Actuators B*, 191 (2014) 508.
47. A. Kaidarova, M. A. Khan, M. Marengo, L. Swanepoel, A. Przybysz, C. Muller, A. Fahlman, U. Buttner, N. R. Gerald, R. P. Wilson, C. M. Duarte, J. Kosel, *npj Flexible Electronics*, 3 (2019) 15.
48. H. Huang, S. Su, N. Wu, H. Wan, S. Wan, H. Bi, L. Sun, *Frontiers in Chemistry*, 7 (2019).

49. T. Han, A. Nag, R. B. V. B. Simorangkir, N. Afsarimanesh, H. Liu, S. C. Mukhopadhyay, Y. Xu, M. Zhadobov, R. Sauleau, *Sensors (Basel)*, 19 (2019) 3477.
50. H. Xu, Y. F. Lu, J. X. Xiang, M. K. Zhang, Y. J. Zhao, Z. Y. Xie, Z. Z. Gu, *Nanoscale*, 10 (2018) 2090.
51. F. Xu, X. Li, Y. Shi, L. Li, W. Wang, L. He, R. Liu, *Micromachines (Basel)*, 9 (2018) 580.
52. K. Shimada, H. Kikura, H. Takahashi, R. Ikeda, *Sensors*, 19 (2019) 689.
53. R. Garg, N. K. Dutta, N. R. Choudhury, *Nanomaterials*, 4 (2014) 267.
54. K. S. Karimov, Z. Ahmad, M. I. Khan, K. J. Siddiqui, T. A. Qasuria, S. Z. Abbas, M. Usman, A.-U. Rehman, *Heliyon*, 5 (2019) e01187.
55. H. Kasim, *Periodica Polytechnica Chemical Engineering*, 63 (2019) 160.

© 2020 The Authors. Published by ESG ([www.electrochemsci.org](http://www.electrochemsci.org)). This article is an open access article distributed under the terms and conditions of the Creative Commons Attribution license (<http://creativecommons.org/licenses/by/4.0/>).